NISAR Time-Series Ratio Algorithm for Soil Moisture Retrieval: Prelaunch Evaluation With SMAPVEX12 Field Campaign Data

Jeonghwan Park, *Member, IEEE*, Rajat Bindlish, *Senior Member, IEEE*, Alexandra Bringer, *Member, IEEE*, Dustin Horton, *Graduate Student Member, IEEE*, and Joel T. Johnson, *Fellow, IEEE*

***Abstract*—The NASA ISRO synthetic aperture radar (NISAR) mission scheduled for launch in 2024 will provide global L-band radar observations that can be applied to estimate land surface soil moisture. The mission's soil moisture product will be provided at 200-m resolution with a global revisit frequency of 12 days (or 6 days when considering both ascending and descending observations). A time-series ratio algorithm for soil moisture retrieval has been applied to NISAR simulated datasets from airborne UAVSAR measurements in the SMAPVEX12 field campaign. Soil moisture retrieval performance using the algorithm is encouraging, with a correlation coefficient between retrievals and in situ observations greater than 0.7 and an unbiased root-mean-squared Error (RMSE) of 0.05 m^3/m^3. The results suggest that the time-series ratio algorithm will provide soil moisture products that meet an accuracy goal of 0.06 m^3/m^3 unbiased RMSE.**

***Index Terms*—NASA ISRO synthetic aperture radar (NISAR) mission, satellite remote sensing, soil moisture retrieval, synthetic aperture radar (SAR), time-series ratio method.**

I. Introduction

SOIL moisture is a critical climate parameter in the Earth's terrestrial hydrology. It plays a significant role in regulating the exchange of water and heat energy between the land surface and atmosphere, primarily through processes, such as evaporation and plant transpiration [1], [2], [3]. Soil moisture information is essential for accurate weather prediction and has further applications in agricultural monitoring, reservoir management, drought and flood forecasting, and other activities related to the management of natural resources.

Significant advancements have occurred over the last decade in satellite remote sensing of soil moisture, largely due to the success of the soil moisture and ocean salinity (SMOS) [4], [5] and soil moisture active and passive (SMAP) [6], [7] missions. These missions use L-band passive microwave measurements to provide soil moisture estimates at 2–3 day intervals having unbiased root-mean-squared error (RMSE) better than 0.04 m^3/m^3. The coarse spatial resolution of the SMOS and SMAP soil moisture products (approximately 36 km), however, limits their use for field-scale agricultural monitoring, which typically requires a spatial resolution of 1 km or finer. Despite the initial intention of SMAP to provide soil moisture retrievals at a 3-km resolution using L-band multipolarization radar observations [8], the radar's failure after three months of operation restricted the achievable results [9]. To achieve finer spatial resolution for soil moisture retrieval, past works have explored the use of high-resolution synthetic aperture radar (SAR), such as Sentinel satellite data [10], [11], [12]. SAR data have also been utilized to downscale other soil moisture products to smaller spatial scales [13], [14].

The NISAR (NASA ISRO Synthetic Aperture Radar) mission scheduled for launch in 2024 [15], [16], [17] will perform L- (1.26 GHz) and S-band (3.2 GHz) backscatter measurements using a sweep SAR approach for a range of remote sensing applications. NISAR will provide global coverage at L-band (up to 80-MHz bandwidth) and limited spatial coverage at S-band (up to 75-MHz bandwidth). The NISAR L-band radar is designed to achieve a 240-km swath width, providing 12-day exact revisit sampling and a spatial resolution that can vary from 3 to 10 m depending on the observing mode. NISAR's incidence angle will range from 34° to 48° across the swath, and it is expected that its fully polarimetric measurements will achieve a noise-equivalent sigma-0 (NES0) better than -20 dB. The NISAR mission will offer the first opportunity for a fine spatial resolution (200-m field-scale) L-band soil moisture product at a frequent revisit rate (as compared to previous L-band SAR missions having greater revisit intervals [18], [19]). This improvement holds great potential for multiple applications. NISAR's L-band frequency further allows for substantial penetration into vegetated regions, enabling frequent revisit measurement of soil moisture even in vegetated areas [20].

Soil moisture retrieval from backscatter data primarily involves inverting a radar forward scattering model that is developed empirically, semiempirically, or theoretically [21], [22],

Manuscript received 24 March 2024; revised 29 May 2024; accepted 15 June 2024. Date of publication 4 July 2024; date of current version 24 July 2024. *(Corresponding author: Jeonghwan Park.)*

Jeonghwan Park is with the Global Science and Technology, Inc., Greenbelt, MD 20770 USA, and also with the NASA Goddard Space Flight Center, Greenbelt, MD 20771 USA (e-mail: jeonghwan.park@nasa.gov).

Rajat Bindlish is with the NASA Goddard Space Flight Center, Greenbelt, MD 20771 USA (e-mail: rajat.bindlish@nasa.gov).

Alexandra Bringer is with the KBR Wyle, Houston, TX 77002 USA, and also with the NASA Goddard Space Flight Center, Greenbelt, MD 20771 USA.

Dustin Horton and Joel T. Johnson are with the Department of Electrical and Computer Engineering, The Ohio State University, Columbus, OH 43210 USA, and also with the ElectroScience Laboratory, The Ohio State University, Columbus, OH 43210 USA.

Digital Object Identifier 10.1109/JSTARS.2024.3422071

[23]. Several analytical electromagnetic scattering approximate models are available to represent bare soil surface scattering, including the small perturbation model (SPM), Kirchhoff approximation, the integral equation method (IEM)/advanced integral equation method, and the small slope approximation (SSA). These physical models explain relationships between the dielectric constant of the soil surface (a function of soil moisture and soil texture) and the measured normalized radar cross section (NRCS) in terms of surface roughness parameters, such as the surface rms height and correlation length. Soil moisture can then be estimated by inverting such models combined with a dielectric mixing model that describes the relationship between the surface complex relative permittivity, soil moisture, and soil texture. Other references have considered the use of empirical or semiempirical forward models [24], [25], [26], [27], [28], [29], and have further explored the impact of vegetation [30], [31], [32] and the benefits of polarimetric measurements [33], [34], [35]. Because the measured NRCS is impacted by the confounding effects of varying surface roughness and vegetation beyond the desired soil moisture, the retrieval of soil moisture from radar measurements remains a challenging problem.

Given these factors, the use of a time-series of measurements may also be desirable to improve performance. Such approaches typically operate under the assumption that temporal changes in vegetation properties and surface roughness are small between consecutive radar overpasses, so that changes in NRCS are mainly due to changes in soil moisture [8], [9], [36], [37], [38], [39], [40], [41], [42], [43], [44]. A times-series principal component analysis [45] and InSAR analyses of phase differences between two measurements [46] have also been reported.

This article applies the time-series "ratio" algorithm [41], [42], [43], [44], [47], [48], [49] to mitigate the potential impacts of vegetation and surface roughness. The method offers simplicity and ease of application and does not require a detailed forward land surface scattering model. The performance of the method is assessed using backscatter time-series measurements obtained from the SMAP Validation Experiment 2012 (SMAPVEX12) field campaign in Winnipeg, Manitoba, Canada. Backscatter time-series measurements in the campaign were collected using NASA's airborne L-band UAVSAR instrument. While initial analyses of time series ratio algorithm retrievals for the SMAPVEX12 campaign were previously presented [42], the current article extends these results with a particular focus on preparation for application of the algorithm with NISAR measurements.

II. Time-Series Ratio Algorithm

The backscattered NRCS of land surfaces can be described using

$$\sigma_{pq}^{t} = \sigma_{pq}^{s} e^{-\tau_{pq}} + \sigma_{pq}^{\mathrm{SV}} + \sigma_{pq}^{V} \tag{1}$$

where σ_{pq}^{t} represents the total NRCS in polarization combination pq, σ_{pq}^{s} corresponds to the NRCS of the soil surface, which is subsequently multiplied by the two-way vegetation attenuation factor $e^{-\tau_{pq}}$, $\sigma_{pq}^{\mathrm{SV}}$ denotes scattering interactions that take place between the soil and vegetation, and σ_{pq}^{V} represents backscattering in the vegetation volume. In many L-band scenarios, particularly those involving soil moisture retrieval, the contribution of vegetation volume scattering (σ_{pq}^{V}) can be neglected. This assumption is less applicable for highly vegetated areas, so it should be expected that retrieval accuracy will degrade in such cases. The authors in [49] reported the incorporation of a vegetation attenuation factor in a time-series ratio method for Sentinel-1 soil moisture retrievals at C-band, but this extension is not considered here. If the first term in (1) is dominant, the NRCS becomes

$$\sigma_{pq}^{t} \approx \sigma_{pq}^{s} e^{-\tau_{pq}}. \tag{2}$$

Under the SPM, first-order SSA, or IEM models, σ_{pq}^{s} can be written as a product of separate functions of the surface roughness and surface relative permittivity, with the dependence on permittivity written as $|\alpha_{\mathrm{PP}}|^2$ for PP either HH or VV polarization. The alpha coefficient (α_{PP}) is a function of the dielectric constants of the soil and the incidence angle. For HH polarization, α_{HH} can be expressed as

$$|\alpha_{\mathrm{HH}}| = \left| \frac{\epsilon - 1}{\left(\cos\theta + \sqrt{\epsilon - \sin^2\theta}\right)^2} \right| = |\Gamma_H| \tag{3}$$

where ϵ is the soil relative complex permittivity, θ is the incidence angle, and $|\Gamma_H|$ is the surface Fresnel reflection coefficient in horizontal polarization. For VV polarization, the expression becomes

$$|\alpha_{\mathrm{VV}}| = \left| \frac{(\epsilon - 1)\left[(\epsilon - 1)\sin^2\theta + \epsilon\right]}{\left(\epsilon\cos\theta + \sqrt{\epsilon - \sin^2\theta}\right)^2} \right|. \tag{4}$$

Fig. 1 plots $|\alpha_{\mathrm{HH}}|$and$|\alpha_{\mathrm{VV}}|$, and their relationship with soil moisture for a clay fraction (CF) of 0.2 under the Mironov dielectric mixing model. While various dielectric mixing models have been reported (e.g., Dobson [50], Wang and Schmugge [51], and others [52]), the Mironov model [53] was created to be applicable across a broader spectrum of soil types by utilizing a more extensive soil database. The model also requires fewer input parameters (specifically, CF and frequency) in comparison to other models, and is used for soil moisture retrieval for both the SMOS and SMAP missions. Both alpha functions monotonically increase with soil moisture, with VV polarization showing a greater increase than that for HH polarization.

The time-series ratio method assumes that the influences of vegetation and surface roughness remain nearly constant between two successive observations, provided that the incidence angle remains unchanged. The ratio of NRCS values at time t_1 and t_2 can then be approximated as

$$\frac{\sigma_{\mathrm{PP}}^{0}(t_2)}{\sigma_{\mathrm{PP}}^{0}(t_1)} \approx \left| \frac{\alpha_{\mathrm{PP}}(t_2,\ \epsilon,\ \theta)}{\alpha_{\mathrm{PP}}(t_1,\ \epsilon,\ \theta)} \right|^2, \quad \mathrm{PP} = \mathrm{HH}\ or\ \mathrm{VV} \tag{5}$$

since any multiplicative vegetation or surface roughness effects cancel when the ratio is taken. Note for HH polarization

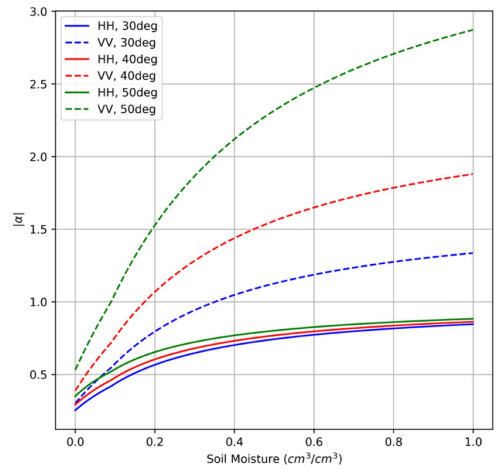

(a)

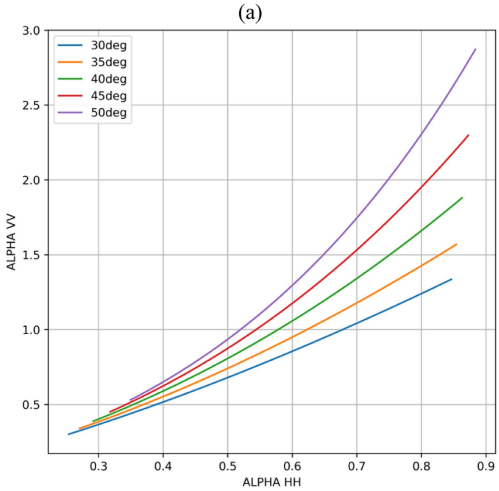

(b)

Fig. 1. (a) $|\alpha_{\mathrm{HH}}|$ and $|\alpha_{\mathrm{VV}}|$, (b) the relationship between $|\alpha_{\mathrm{HH}}|$ and $|\alpha_{\mathrm{VV}}|$ with various incidence angles from 30° to 50°. The Mironov model is used in this analysis and CF is fixed at 0.2 and the first-order SPM scattering model is utilized for this simulation.

this assumption holds regardless of whether surface scattering, surface-vegetation interactions, or a combination dominates scattering, because all terms are proportional to the horizontally polarized reflection coefficient. This is not true for VV polarization because $|\alpha_{\mathrm{VV}}|$ is distinct from the vertically polarized Fresnel reflection coefficient. With a time series of N NRCS observations, *N*-1 ratios can be computed and combined into a matrix equation

$$\begin{bmatrix} 1 & -\sqrt{\frac{\sigma^0_{\mathrm{PP}}(t_1)}{\sigma^0_{\mathrm{PP}}(t_2)}} & \cdots & 0 & 0 \\ 0 & 1 & & 0 & 0 \\ \vdots & & \ddots & & \vdots \\ 0 & 0 & \cdots & 1 & -\sqrt{\frac{\sigma^0_{\mathrm{PP}}(t_{N-1})}{\sigma^0_{\mathrm{PP}}(t_N)}} \\ 0 & 0 & & 0 & 1 \end{bmatrix} \begin{bmatrix} |\alpha_{\mathrm{PP}}(t_1)| \\ |\alpha_{\mathrm{PP}}(t_2)| \\ \vdots \\ |\alpha_{\mathrm{PP}}(t_N)| \end{bmatrix} = \begin{bmatrix} 0 \\ 0 \\ \vdots \\ 0 \end{bmatrix} \tag{6}$$

where PP can be either HH or VV polarization. Since the linear equation has no constant term, the right-hand side entries are zeros. Because the matrix equation is not fully determined, additional ancillary information is required to obtain a solution. There are a variety of methods that can be considered for applying ancillary information to complete the solution. In what follows, maximum and minimum allowed alpha coefficients over the time series are used. A bounded linear least-squares solution of the *N*-1 by *N* matrix equation can then be applied to obtain the alpha coefficients at each time step from which inversion of the dielectric mixing model and alpha coefficient equation provides soil moisture. The method can also be extended if both HH and VV polarized measurements are available. In what follows, separate inversions for HH and VV polarized alpha coefficients are performed, and the two alpha values are used in a combined estimation of a single soil moisture value. The combination identifies an index

$$i_{\mathrm{HH+VV}} = \underset{i}{\operatorname{argmin}} \left(\left(\alpha_{\mathrm{HH}} - \alpha^T_{\mathrm{HH}}(i)\right)^2 + \left(\alpha_{\mathrm{VV}} - \alpha^T_{\mathrm{VV}}(i)\right)^2 \right) \tag{7}$$

in a precomputed look-up table $\alpha^T_{\mathrm{HH}}(i)$ and $\alpha^T_{\mathrm{VV}}(i)$ given the soil texture and incidence angle conditions of a particular observation. Specifically, the α_{HH} and α_{VV} values at a particular time step obtained through individual HH and VV retrievals are used in (7) to find a soil moisture index that minimizes the cost function. Based on this index, the corresponding soil moisture value can then be determined. The $i_{\mathrm{HH+VV}}$ index is computed for any point in the time series for which HH and VV polarized alpha information are both available.

The length of the time series used must also be considered because the method implicitly assumes that roughness and vegetation changes remain modest over the entire time series. Given NISAR's 6 to 12 day revisit cycle, a 3-point time series is initially planned. It is noted that over the corresponding 24-day interval, vegetation structure may change significantly during the growing or harvest seasons in agricultural areas. However, several studies, including [42], have demonstrated that the method can detect soil moisture changes even in the presence of substantial vegetation change. The results to be shown also indicate this potential, given the highly varying vegetation conditions of the SMAPVEX12 dataset.

III. SMAPVEX12 Data Analysis

Prelaunch algorithm implementation and validation tests were performed for the SMAP Validation Experiment 2012 (SMAPVEX12- conducted near Winnipeg, Manitoba, Canada) field campaign in which NASA's airborne L-band UAVSAR instrument acquired measurements [54].

Fig. 2 shows the entire SMAPVEX12 study area, which included 55 agricultural and 4 forest in-situ sites at which ground data were collected in June and July 2012. Agricultural sites included fields used for soybean, corn, wheat, oat, and canola crops, along with multiple pasture sites. UAVSAR observations were acquired in multiple flights from June 17 to July 17, 2012. UAVSAR's fully polarimetric L-band (1.26 GHz) radar provides ~7-m resolution in its multilooked ground-range projected

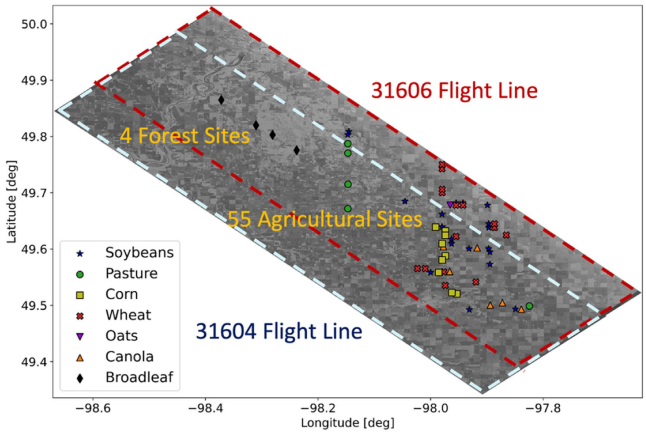

Fig. 2. SMAMVEX12 study areas with 55 agricultural (soybeans, pasture, corn, wheat, oats, canola) and 4 forest sites around Winnipeg in Canada. There are two UAVSAR flight lines (31604 and 31606).

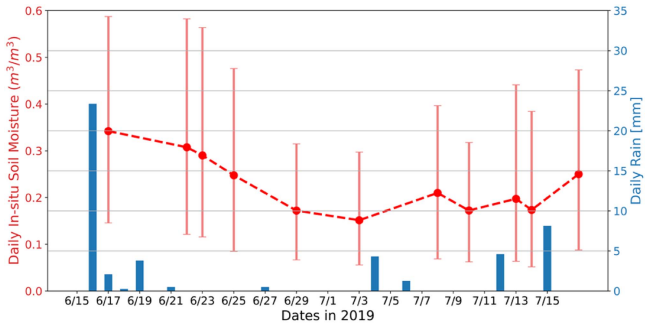

Fig. 3. Precipitation data obtained from seven weather stations around the study area (blue bar indicates daily rain amount in mm) and daily in-situ soil moisture information (red dashed line indicates the daily average of in-situ soil moistures from all sites with daily soil moisture min/max values for 11 days of UAVSAR measurements).

(GRD) product at incidence angles between 20° and 70° [55]. The two UAVSAR flight lines (31604 and 31606) shown in Fig. 2 are examined in what follows, each having 11 and 14 flights, respectively. The common 11 flights of each flight line are considered in this analysis. The NISAR project reprocessed UAVSAR data into a NISAR-like configuration (HH 20-MHz bandwidth and VV 5MHz-bandwidth) that was aggregated to 200-m resolution for soil moisture retrievals. UAVSAR measurements within the incidence angle range 30° to 50° were further used for consistency with the NISAR mission. For the in-situ sites, ancillary data including soil texture, land cover, and vegetation water content (VWC) are available in addition to soil moisture measurements.

Fig. 3 plots daily precipitation data (average from seven weather stations in the study area) and average in-situ soil moisture measurements. There are significant rain events on June 16, July 4, July 12, and July 15 that impact daily in-situ soil moistures. The average soil moisture was highest at the start of the experiment on June 17 followed by a dry down from June 21 to July 3. Soil moisture then increases after precipitation events on July 4, 12, and 15.

Minimum and maximum alpha bounds were estimated using soil texture information at each pixel, in contrast to [42] which used minimum and maximum in-situ values at each location. Use of soil texture-derived bounds avoids the need for local soil moisture information. Ancillary soil texture information, including CF, bulk density, sand fraction, and organic content (OC), is available from the in-situ locations and was used to derive a single second order fit to the minimum and maximum in-situ measured soil moistures from all available sites. The derived regression model was then used to determine the upper and lower bounds of soil moisture at each site based on soil texture information. These site-specific soil moisture bounds were then transformed into the alpha bounds used in soil moisture retrieval by using the lookup table combined with incidence angle and CF information.

IV. Results and Discussion

A. Alpha Ratios Versus Backscatter Ratios

The algorithm relies on the assumption that the ratio of consecutive backscatter measurements is identical to the corresponding ratio of alpha coefficients. Fig. 4 plots these ratios for both HH and VV polarizations at multiple field sites using in-situ soil moisture information to obtain the ratio of alpha coefficients. Fig. 4(a) and (b) present examples (soybean and wheat fields) showing measurements that lie near the desired 1:1 line. The results in Fig. 4(c) and (d) are somewhat similar but show a greater presence of outliers, while those in Fig. 4(e) and (f) show worse results. These results are provided to illustrate the basic concept of the algorithm (which was applied identically for all field sites) and the benefits of introducing ancillary maximum and minimum bounds. These results also suggest future opportunities for further algorithm improvements not considered here, for example based on "rescaling" the retrieval by comparing maximum to minimum NRCS ratios to those of the ancillary maximum and minimum alpha coefficients.

B. Performance Comparison Between Two Flight Lines

The two UAVSAR flight lines considered include a narrow overlap area within the 30° to 50° incidence angle range that includes seven agricultural in-situ sites. Fig. 5 compares the two retrievals with in-situ measurements at sites 14 (soybeans) and 24 (corn) using combined HH+VV retrievals. For these example sites, the incidence angles are 31° to 34° for the 31604 flight line and 49° to 50° for the 31606 flight line, respectively. The retrieval time series from each flight line are similar with difference less than 0.05 m^3/m^3 and good agreement with in-situ measurements is also observed, (although a few days show differences up to 0.1 m^3/m^3). The soybean site shows an unbiased RMSE of 0.034 m^3/m^3 for the 31604 flight line and 0.036 m^3/m^3 for the 31606 flight line, whereas the corn site exhibits values of 0.049 m^3/m^3 for the 31604 flight line and 0.034 m^3/m^3 for the 31606 flight line. Fig. 6 further provides a histogram of retrieval differences between two flight lines over common areas for the HH+VV combination. The results show a mean difference of 0.002 m^3/m^3 and standard deviation of

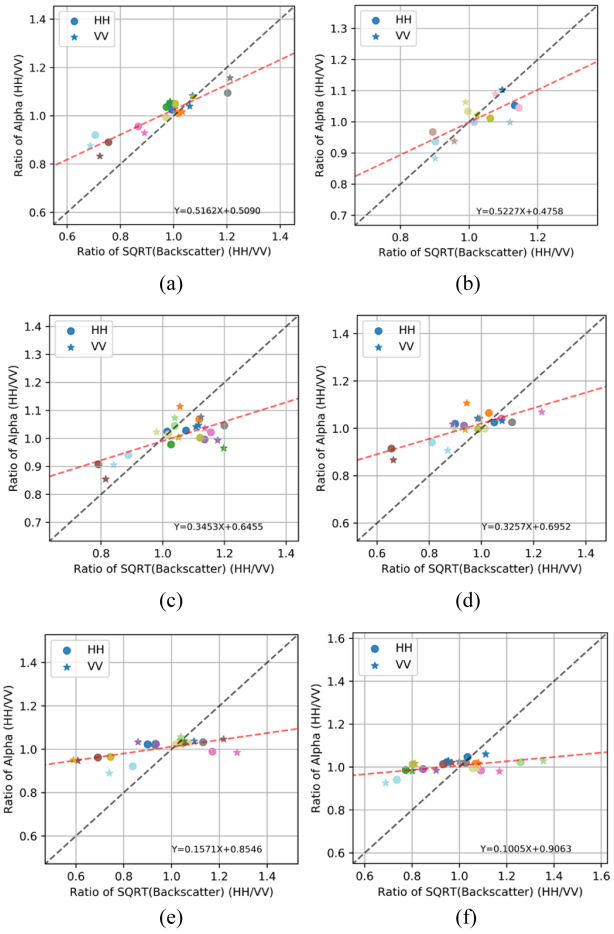

Fig. 4. Relationship between consecutive backscatter measurement (HH and VV) ratios and the corresponding alpha ratios. (a) Site 111 (soybeans). (b) Site 85 (wheat). (c) Site 61 (canola). (d) Site 62 (corn). (e) Site 51 (soybeans). (f) Site 11 (corn). All measurements from flight line 31606 and red dashed curves indicate a linear fit.

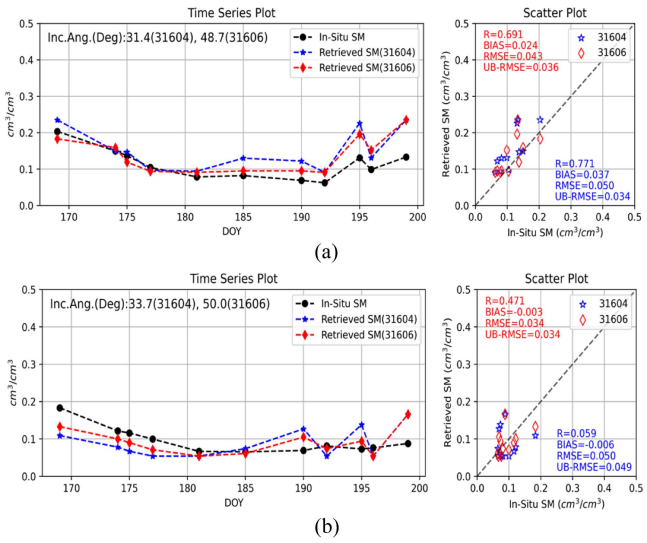

Fig. 5. Performance comparison at sites 14 (soybeans) and 24 (corn) where retrievals from both flight lines are available. HH+VV configuration used for this comparison. (a) Site 14 (Soybeans). (b) Site 24 (Corn).

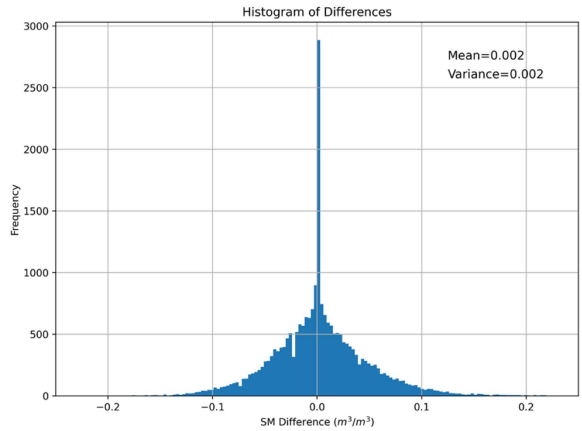

Fig. 6. Histogram of the retrieval (HH+VV) difference between 31 604 and 31 606 flight line over common areas. Data at seven agricultural sites for 11 days was used.

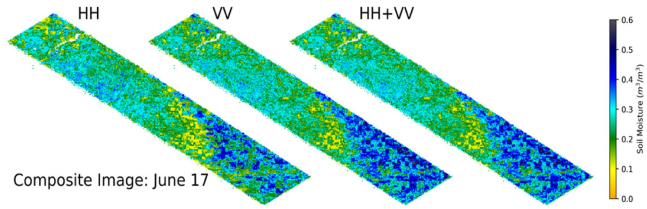

Fig. 7. Estimated composite soil moisture images on June 17 (the first day of UAVSAR experiment) using the time-series ratio algorithm for HH, VV, and HH+VV configuration.

0.0447 m^3/m^3, demonstrating the overall agreement in the soil moisture retrieval for the two flight lines.

C. Composite Image Generation

Soil moisture retrievals were obtained for each polarization by solving the matrix equation with the soil texture based alpha bounds. Fig. 7 illustrates retrieved soil moisture images on June 17, the first day of the UAVSAR experiment. Composite images were produced by combining soil moisture retrievals from both flight lines, with the average soil moisture for the two flight lines used in the overlap area. Retrievals were not performed for pixels with invalid soil texture information, such as those in river and urban areas. From the image, the HH+VV, HH, and VV-based soil moisture images are similar, but have small differences depending on the method.

Fig. 8 provides HH+VV retrieved soil moisture images for the entire time series. The SMAPVEX12 field experiment started on June 17 after a heavy rain, so that the average in-situ soil moisture was high on June 17. Only light precipitation events then occurred until June 23. Agricultural areas in the southern part of the domain show particularly high soil moisture values in this time interval. Soil moisture then decreased throughout the domain until July 3. Subsequent rain events on July 4, 12, and 14 then caused higher soil moistures in the region. The retrieved images are largely consistent with these trends and with the averaged in-situ soil moistures shown in Fig. 3. The images

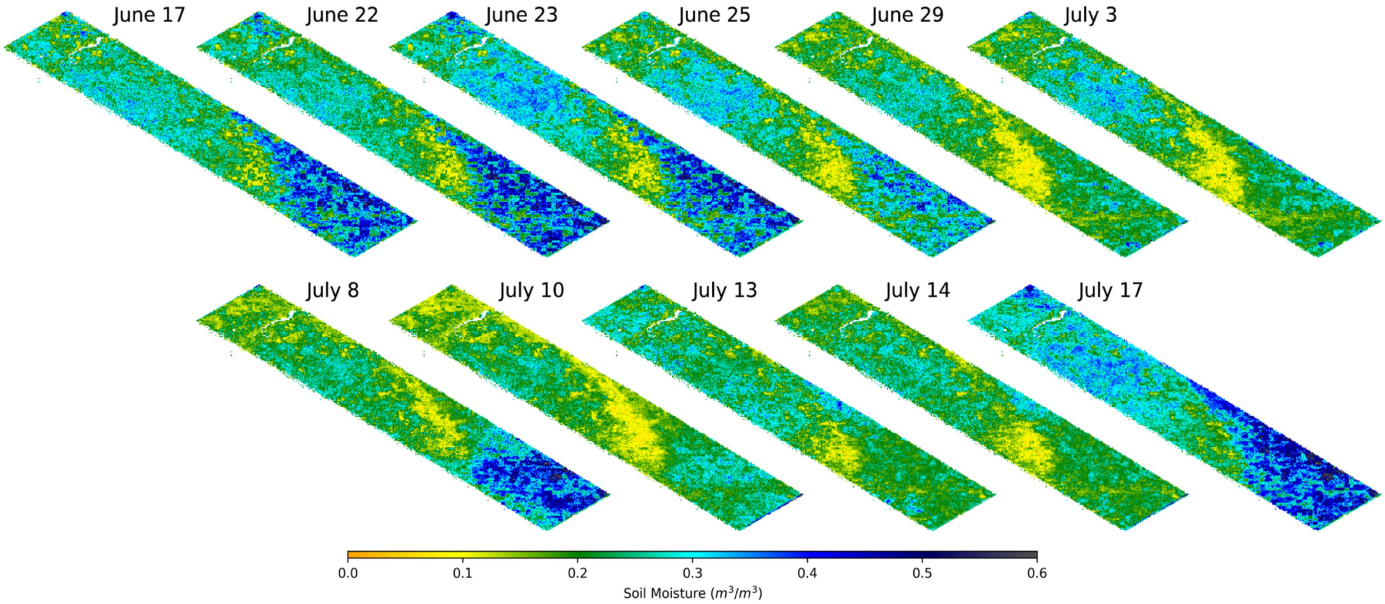

Fig. 8. Composite retrieved soil moisture images from June 17 to July 17, 2012, with HH+VV configuration. 11 common flight lines of 31604 and 31606 were used for the images.

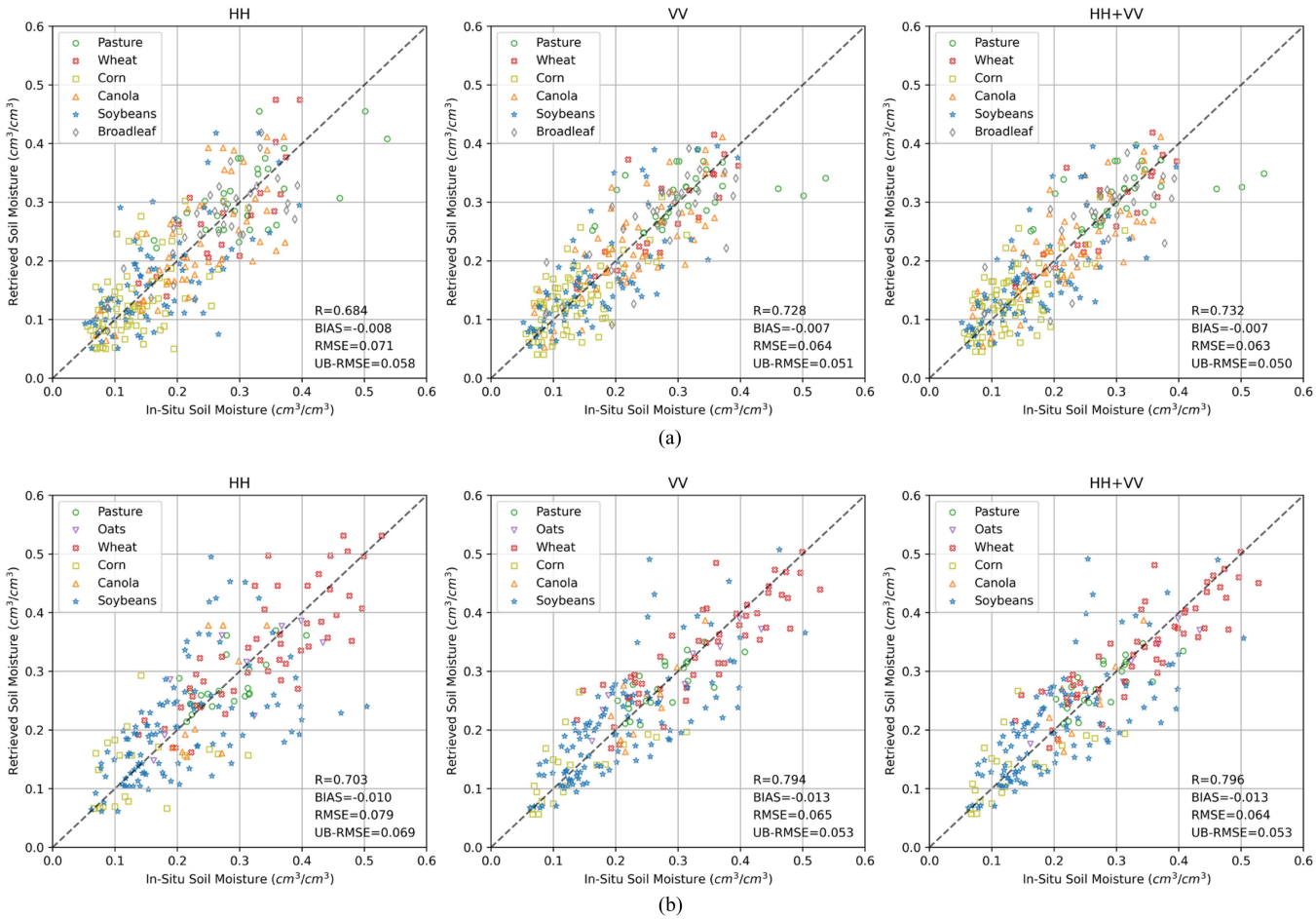

Fig. 9. Scatter plots between in-situ soil moistures and retrieved soil moistures for HH, VV, and HH+VV combination. (a) 31604 Flight Line. (b) 31606 Flight Line.

TABLE I
PERFORMANCE STATISTICS PER CROP AND PER POLARIZATION (SITE-BASED BIAS CORRECTION)

(A) 31604 FLIGHT LINE

31604 Flight Line		Pasture	Wheat	Corn	Canola	Soybeans	Broadleaf	Total	Agricultural Sites Total
Sample Number		31	20	73	59	74	36	293	226
HH	R	0.614	0.788	0.477	0.724	0.650	-0.022	0.684	0.722
	Bias	-0.062	-0.010	0.001	-0.013	0.018	-0.018	-0.008	0.001
	RMSE	0.088	0.055	0.056	0.063	0.078	0.096	0.071	0.064
	UB-RMSE	0.058	0.051	0.054	0.061	0.066	0.050	0.058	0.059
VV	R	0.408	0.802	0.479	0.752	0.746	0.156	0.728	0.769
	Bias	-0.059	-0.013	0.000	-0.014	0.008	0.011	-0.007	-0.003
	RMSE	0.087	0.047	0.052	0.057	0.066	0.083	0.064	0.057
	UB-RMSE	0.058	0.044	0.044	0.051	0.057	0.052	0.051	0.050
HH+VV	R	0.462	0.823	0.497	0.762	0.736	0.148	0.732	0.771
	Bias	-0.060	-0.013	0.000	-0.015	0.009	0.007	-0.007	-0.003
	RMSE	0.087	0.045	0.051	0.056	0.067	0.082	0.063	0.056
	UB-RMSE	0.057	0.041	0.044	0.050	0.058	0.050	0.050	0.049

(B) 31606 FLIGHT LINE

31606 Flight Line		Pasture	Oats	Wheat	Corn	Canola	Soybeans	Total	Agricultural Sites Total
Sample Number		22	9	50	21	10	106	218	196
HH	R	0.496	0.755	0.780	0.092	0.726	0.470	0.703	0.716
	Bias	-0.052	0.005	-0.013	-0.034	0.021	-0.001	-0.010	-0.006
	RMSE	0.073	0.063	0.066	0.084	0.073	0.089	0.079	0.079
	UB-RMSE	0.040	0.063	0.056	0.076	0.070	0.082	0.069	0.072
VV	R	0.603	0.936	0.758	0.548	0.822	0.667	0.794	0.799
	Bias	-0.032	-0.007	-0.028	-0.021	0.012	-0.001	-0.013	-0.011
	RMSE	0.054	0.041	0.070	0.058	0.038	0.070	0.065	0.066
	UB-RMSE	0.036	0.040	0.052	0.053	0.036	0.061	0.053	0.055
HH+VV	R	0.604	0.941	0.783	0.522	0.838	0.656	0.796	0.802
	Bias	-0.034	-0.006	-0.027	-0.022	0.012	-0.002	-0.013	-0.011
	RMSE	0.055	0.040	0.067	0.059	0.037	0.071	0.064	0.065
	UB-RMSE	0.034	0.039	0.050	0.054	0.035	0.062	0.053	0.055

further show a greater variability in soil moisture in southern agricultural areas as compared to the more northern forest areas.

D. Assessment With In-Situ Measurements

Fig. 9 provides scatter plots comparing retrieved and in-situ site soil moistures using all data for each flight line, and for the HH-only, VV-only, and combined retrievals. Each crop type is marked with a separate color and symbol in the figure. Sites 101–105 had standing water during the experiment and were not used in the performance assessment. Statistics including the correlation coefficient (R), bias, RMSE, and unbiased RMSE are indicated at the bottom of each figure. Biases for each in-situ site were removed in the scatter plot and in computing performance excepting the mean bias. Both flight lines show overall reasonable performance for all the methods. The HH+VV combination generally outperforms individual polarizations with an unbiased RMSE of 0.050 m^3/m^3 and a correlation coefficient of 0.732 for flight line 31604. For flight line 31606, it achieves an unbiased RMSE of 0.053 m^3/m^3 and a correlation coefficient of 0.796. The VV-only results further show reduced errors as compared to HH-only due to the enhanced sensitivity to soil moisture in VV polarization.

Soil moisture retrievals from the SMAP radar using a physical model inversion method with time-series data achieved an RMSE of 0.052 m^3/m^3 across all SMAP validation sites in [9]. This level of accuracy is comparable to that found here for the SMAPVEX12 dataset. However, the auhtors in [9] also reported an average bias of -0.015 m^3/m^3 and a correlation coefficient of 0.50, both degraded as compared to the SMAPVEX12 results reported here.

The percent unbiased RMSE was also calculated to understand relative errors. It is a normalized metric that expresses the error as a percentage of the mean of the observed values.

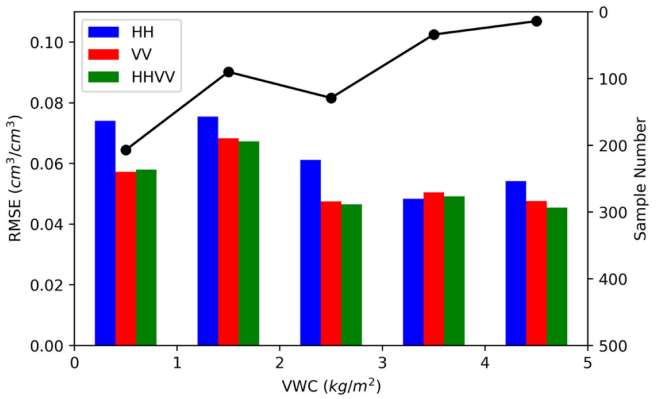

Fig. 10. Performance comparison by various VWC ranges for all polarizations (HH, VV, and HH+VV); Number of samples for each VWC class are indicated with a line graph on the secondary axis.

For flight line 31604, the percent unbiased RMSEs are 28.29%, 24.98%, and 24.64% for HH, VV, and HH+VV polarizations, respectively. For flight line 31606, these values are 28.49%, 22.06%, and 21.90%. The percent unbiased RMSE has a relatively higher value since it is influenced by the mean soil moisture, which ranges from 0.05 to 0.54 m^3/m^3 over the campaign. Errors in areas with lower soil moisture particularly can increase the relative RMSE.

The results are also based on the NISAR-like backscatter data (both HH and VV) with 200-m aggregation. Retrievals at finer spatial resolution could also be attempted, but would be impacted by increased levels of speckle noise that would degrade performance.

Table I presents performance statistics per crop and polarization in detail. Results for oats, wheat, corn, and canola show overall reasonable performance (HH+VV) with unbiased RMSE less than 0.050 m^3/m^3. Performance is more variable for soybeans, with unbiased RMSE varying from 0.058 to 0.062 m^3/m^3 depending on the method used. This may be indicative of more significant contributions from vegetation volume scattering for the soybean crop type. The correlation coefficients for oats, wheat, and canola across both flight lines are found to be relatively high, with values exceeding 0.72 for all cases. However, forest sites show low correlations due to the small dynamic range in soil moisture for the forest sites. Also, the bias for the pasture sites is larger than that for other crop types. The table also provides statistics specifically for agricultural sites in the last column and the results illustrate robust soil moisture retrieval across various agricultural sites, with correlations surpassing 0.75 and demonstrating low unbiased RMSE values, highlighting the effectiveness of the employed methodology.

E. Impact of Vegetation Water Content

Fig. 10 examines soil moisture retrieval errors as a function of in-situ VWC for each polarization configuration. The results show similar retrieval errors over the 0–5 $\mathrm{kg/m^2}$ VWC range considered that are consistent for all crop types. These results suggest that low to moderate vegetation levels should not be expected to have a significant impact on time-series ratio algorithm performance, although this conclusion may be influenced by the particular vegetation types and conditions of the SMAPVEX12 experiment. Further assessment over a larger range of conditions will be possible once NISAR mission data is available.

V. Conclusion

A time-series ratio method for soil moisture retrieval was successfully applied to the NISAR simulated SMAPVEX12 UAVSAR data. The method shows a reasonable performance with unbiased RMSE of 0.05 m^3/m^3 and appears suitable for use for the NISAR mission. The method is advantageous since it does not require any forward modeling of the backscattered NRCS. Also, because minimal ancillary data are needed, the method is less sensitive to errors in ancillary data. The results obtained showed better retrieval performance for VV as compared to HH polarization, with the combined HH+VV retrieval showing the best performance.

Future work will consider the incorporation of cross-pol observations to flag areas having appreciable changes in vegetation between consecutive overpasses. To facilitate global soil moisture processing in the NISAR mission, the use of a climatological data in determining minimum and maximum alpha coefficient bounds is also under development. Combined L- and S-band retrievals are also under consideration to further support the simultaneous estimation of vegetation water content and/or biomass.

References

[1] S. I. Seneviratne et al., "Investigating soil moisture–climate interactions in a changing climate: A review," *Earth-Sci. Rev.*, vol. 99, no. 3/4, pp. 125–161, 2010.
[2] V. Klemas, C. W. Finkl, and N. Kabbara, "Remote sensing of soil moisture: An overview in relation to coastal soils," *J. Coastal Res.*, vol. 30, no. 4, pp. 685–696, 2014.
[3] T. Oki and S. Kanae, "Global hydrological cycles and world water resources," *Science*, vol. 313, no. 5790, pp. 1068–1072, 2006.
[4] H. M. J. P. Barré, B. Duesmann, and Y. H. Kerr, "SMOS: The mission and the system," *IEEE Trans. Geosci. Remote Sens.*, vol. 46, no. 3, pp. 587–593, Mar. 2008.
[5] Y. H. Kerr et al., "The SMOS mission: New tool for monitoring key elements of the global water cycle," *Proc. IEEE*, vol. 98, no. 5, pp. 666–687, May 2010.
[6] D. Entekhabi et al., "The soil moisture active passive (SMAP) mission," *Proc. IEEE*, vol. 98, no. 5, pp. 704–716, May 2010.
[7] S. K. Chan et al., "Assessment of the SMAP passive soil moisture product," *IEEE Trans. Geosci. Remote Sens.*, vol. 54, no. 8, pp. 4994–5007, Aug. 2016.
[8] S.-B. Kim, L. Tsang, J. T. Johnson, S. Huang, J. J. van Zyl, and E. G. Njoku, "Soil moisture retrieval using time-series radar observations over bare surfaces," *IEEE Trans. Geosci. Remote Sens.*, vol. 50, no. 5, pp. 1853–1863, May 2012.
[9] S.-B. Kim et al., "Surface soil moisture retrieval using the L-band synthetic aperture radar onboard the soil moisture active–passive satellite and evaluation at core validation sites," *IEEE Trans. Geosci. Remote Sens.*, vol. 55, no. 4, pp. 1897–1914, Apr. 2017.
[10] S. Zwieback and A. A. Berg, "Fine-scale SAR soil moisture estimation in the subarctic tundra," *IEEE Trans. Geosci. Remote Sens.*, vol. 57, no. 7, pp. 4898–4912, Jul. 2019.

[11] S. Paloscia, S. Pettinato, E. Santi, C. Notarnicola, L. Pasolli, and A. Reppucci, "Soil moisture mapping using Sentinel-1 images: Algorithm and preliminary validation," *Remote Sens. Environ.*, vol. 134, pp. 234–248, 2013.

[12] M. E. Hajj, N. Baghdadi, M. Zribi, and H. Bazzi, "Synergic use of Sentinel-1 and Sentinel-2 images for operational soil moisture mapping at high spatial resolution over agricultural areas," *Remote Sens.*, vol. 9, no. 12, 2017, Art. no. 1292.

[13] N. N. Das et al., "High-resolution enhanced product based on SMAP active-passive approach using Sentinel 1A and 1B SAR data," in *Proc. IEEE Int. Geosci. Remote Sens. Symp.*, 2017, pp. 2543–2545.

[14] J. Peng, A. Loew, O. Merlin, and N. E. C. Verhoest, "A review of spatial downscaling of satellite remotely sensed soil moisture," *Rev. Geophys.*, vol. 55, no. 2, pp. 341–366, 2017.

[15] P. Rosen et al., "The NASA-ISRO SAR (NISAR) mission dual-band radar instrument preliminary design," in *Proc. IEEE Int. Geosci. Remote Sens. Symp.*, 2017, pp. 3832–3835.

[16] "NASA-IRSO SAR (NISAR) mission science users' handbook, version 1," NASA Jet Propulsion Lab., Pasadena, CA, USA, 2018.

[17] "NISAR calibration and validation plan, V0.9," NASA Jet Propulsion Lab., Pasadena, CA, USA, 2018.

[18] Y. Kojima, K. Oki, K. Noborio, and M. Mizoguchi, "Estimating soil moisture distributions across small farm fields with ALOS/PALSAR," *Int. Scholarly Res. Notices*, vol. 2016, 2016, Art. no. 4203783.

[19] T. Motohka, O. Isoguchi, M. Sakashita, and M. Shimada, "Results of ALOS-2 PALSAR-2 calibration and validation after 3 years of operation," in *Proc. IEEE Int. Geosci. Remote Sens. Symp.*, 2018, pp. 4169–4170.

[20] P. S. Narvekar, D. Entekhabi, S.-B. Kim, and E. G. Njoku, "Soil moisture retrieval using L-band radar observations," *IEEE Trans. Geosci. Remote Sens.*, vol. 53, no. 6, pp. 3492–3506, Jun. 2015.

[21] N. E. C. Verhoest, H. Lievens, W. Wagner, J. Álvarez-Mozos, M. S. Moran, and F. Mattia, "On the soil roughness parameterization problem in soil moisture retrieval of bare surfaces from synthetic aperture radar," *Sensors*, vol. 8, no. 7, pp. 4213–4248, 2008.

[22] G. P. Petropoulos, G. Ireland, and B. Barrett, "Surface soil moisture retrievals from remote sensing: Current status, products & future trends," *Phys. Chem. Earth, Parts A/B/C*, vol. 83, pp. 36–56, 2015.

[23] B. Barrett, E. Dwyer, and P. Whelan, "Soil moisture retrieval from active spaceborne microwave observations: An evaluation of current techniques," *Remote Sens.*, vol. 1, no. 3, pp. 210–242, 2009.

[24] A. Quesney et al., "Estimation of watershed soil moisture index from ERS/SAR data," *Remote Sens. Environ.*, vol. 72, no. 3, pp. 290–303, 2000.

[25] S. Chatterjee, J. Huang, and A. E. Hartemink, "Establishing an empirical model for surface soil moisture retrieval at the U.S. climate reference network using Sentinel-1 backscatter and ancillary data," *Remote Sens.*, vol. 12, no. 8, 2020, Art. no. 1242.

[26] E. Santi, S. Paloscia, S. Pettinato, L. Brocca, L. Ciabatta, and D. Entekhabi, "On the synergy of SMAP, AMSR2 AND SENTINEL-1 for retrieving soil moisture," *Int. J. Appl. Earth Observation Geoinf.*, vol. 65, pp. 114–123, 2018.

[27] Y. Oh, K. Sarabandi, and F. T. Ulaby, "An empirical model and an inversion technique for radar scattering from bare soil surfaces," *IEEE Trans. Geosci. Remote Sens.*, vol. 30, no. 2, pp. 370–381, Mar. 1992.

[28] P. C. Dubois, J. van Zyl, and T. Engman, "Measuring soil moisture with imaging radars," *IEEE Trans. Geosci. Remote Sens.*, vol. 33, no. 4, pp. 915–926, Jul. 1995.

[29] J. Shi, J. Wang, A. Y. Hsu, P. E. O'Neill, and E. T. Engman, "Estimation of bare surface soil moisture and surface roughness parameter using L-band SAR image data," *IEEE Trans. Geosci. Remote Sens.*, vol. 35, no. 5, pp. 1254–1266, Sep. 1997.

[30] E. P. W. Attema and F. T. Ulaby, "Vegetation modeled as a water cloud," *Radio Sci.*, vol. 13, no. 2, pp. 357–364, 1978.

[31] R. Bindlish and A. P. Barros, "Parameterization of vegetation backscatter in radar-based, soil moisture estimation," *Remote Sens. Environ.*, vol. 76, no. 1, pp. 130–137, 2001.

[32] S.-B. Kim, M. Moghaddam, L. Tsang, M. Burgin, X. Xu, and E. G. Njoku, "Models of L-band radar backscattering coefficients over global terrain for soil moisture retrieval," *IEEE Trans. Geosci. Remote Sens.*, vol. 52, no. 2, pp. 1381–1396, Feb. 2014.

[33] F. Mattia et al., "The effect of surface roughness on multifrequency polarimetric SAR data," *IEEE Trans. Geosci. Remote Sens.*, vol. 35, no. 4, pp. 954–966, Jul. 1997.

[34] D. L. Schuler, J.-S. Lee, D. Kasilingam, and G. Nesti, "Surface roughness and slope measurements using polarimetric SAR data," *IEEE Trans. Geosci. Remote Sens.*, vol. 40, no. 3, pp. 687–698, Mar. 2002.

[35] M. L. Williams, "Potential for surface parameter estimation using compact polarimetric SAR," *IEEE Geosci. Remote Sens. Lett.*, vol. 5, no. 3, pp. 471–473, Jul. 2008.

[36] V. Naeimi, K. Scipal, Z. Bartalis, S. Hasenauer, and W. Wagner, "An improved soil moisture retrieval algorithm for ERS and METOP scatterometer observations," *IEEE Trans. Geosci. Remote Sens.*, vol. 47, no. 7, pp. 1999–2013, Jul. 2009.

[37] L. Brocca, F. Melone, T. Moramarco, W. Wagner, and S. Hasenauer, "ASCAT soil wetness index validation through in situ and modeled soil moisture data in central Italy," *Remote Sens. Environ.*, vol. 114, no. 11, pp. 2745–2755, 2010.

[38] M. Shoshany, T. Svoray, P. J. Curran, G. M. Foody, and A. Perevolotsky, "The relationship between ERS-2 SAR backscatter and soil moisture: Generalization from a humid to semi-arid transect," *Int. J. Remote Sens.*, vol. 21, no. 11, pp. 2337–2343, 2000.

[39] D. P. Thoma et al., "Comparison of four models to determine surface soil moisture from C-band radar imagery in a sparsely vegetated semiarid landscape," *Water Resour. Res.*, vol. 42, no. 1, 2006.

[40] F. Mattia, G. Satalino, V. R. N. Pauwels, and A. Loew, "Soil moisture retrieval through a merging of multi-temporal L-band SAR data and hydrologic modelling," *Hydrol. Earth Syst. Sci.*, vol. 13, no. 3, pp. 343–356, 2009.

[41] A. Balenzano, F. Mattia, G. Satalino, and M. W. J. Davidson, "Dense temporal series of C- and L-band SAR data for soil moisture retrieval over agricultural crops," *IEEE J. Sel. Topics Appl. Earth Observ. Remote Sens.*, vol. 4, no. 2, pp. 439–450, Jun. 2011.

[42] J. D. Ouellette et al., "A time-series approach to estimating soil moisture from vegetated surfaces using L-band radar backscatter," *IEEE Trans. Geosci. Remote Sens.*, vol. 55, no. 6, pp. 3186–3193, Jun. 2017.

[43] L. He, Q. Qin, R. Panciera, M. Tanase, J. P. Walker, and Y. Hong, "An extension of the alpha approximation method for soil moisture estimation using time-series SAR data over bare soil surfaces," *IEEE Geosci. Remote Sens. Lett.*, vol. 14, no. 8, pp. 1328–1332, Aug. 2017.

[44] A. Balenzano et al., "On the use of temporal series of L-and X-band SAR data for soil moisture retrieval. Capitanata plain case study," *Eur. J. Remote Sens.*, vol. 46, no. 1, pp. 721–737, 2017.

[45] N. E. C. Verhoest, P. A. Troch, C. Paniconi, and F. P. D. Troch, "Mapping basin scale variable source areas from multitemporal remotely sensed observations of soil moisture behavior," *Water Resour. Res.*, vol. 34, no. 12, pp. 3235–3244, 1998.

[46] F. de Zan, A. Parizzi, P. Prats-Iraola, and P. López-Dekker, "A SAR interferometric model for soil moisture," *IEEE Trans. Geosci. Remote Sens.*, vol. 52, no. 1, pp. 418–425, Jan. 2014.

[47] M. M. Al-Khaldi, J. T. Johnson, A. J. O'Brien, A. Balenzano, and F. Mattia, "Time-series retrieval of soil moisture using CYGNSS," *IEEE Trans. Geosci. Remote Sens.*, vol. 57, no. 7, pp. 4322–4331, Jul. 2019.

[48] A. Bringer, J. T. Johnson, and R. Bindlish, "Predicting soil moisture retrieval performance for the NISAR mission," in *Proc. IEEE Int. Geosci. Remote Sens. Symp.*, 2020, pp. 4692–4695.

[49] L. Zhu, R. Si, X. Shen, and J. P. Walker, "An advanced change detection method for time-series soil moisture retrieval from Sentinel-1," *Remote Sens. Environ.*, vol. 279, 2022, Art. no. 113137.

[50] M. C. Dobson, F. T. Ulaby, M. T. Hallikainen, and M. A. El-Rayes, "Microwave dielectric behavior of wet soil-part II: Dielectric mixing models," *IEEE Trans. Geosci. Remote Sens.*, vol. GE-23, no. 1, pp. 35–46, Jan. 1985.

[51] J. R. Wang and T. J. Schmugge, "An empirical model for the complex dielectric permittivity of soils as a function of water content," *IEEE Trans. Geosci. Remote Sens.*, vol. GE-18, no. 4, pp. 288–295, Oct. 1980.

[52] R. Zhang, S. Chan, R. Bindlish, and V. Lakshmi, "A performance analysis of soil dielectric models over organic soils in alaska for passive microwave remote sensing of soil moisture," *Remote Sens.*, vol. 15, no. 6, 2023, Art. no. 1658.

[53] V. L. Mironov, L. G. Kosolapova, and S. V. Fomin, "Physically and mineralogically based spectroscopic dielectric model for moist soils," *IEEE Trans. Geosci. Remote Sens.*, vol. 47, no. 7, pp. 2059–2070, Jul. 2009.

[54] H. McNairn et al., "The soil moisture active passive validation experiment 2012 (SMAPVEX12): Prelaunch calibration and validation of the SMAP soil moisture algorithms," *IEEE Trans. Geosci. Remote Sens.*, vol. 53, no. 5, pp. 2784–2801, May 2015.

[55] P. A. Rosen et al., "UAVSAR: A New NASA airbome SAR system for science and technology research," in *Proc. IEEE Conf. Radar*, 2006, pp. 22–29.

Jeonghwan Park (Member, IEEE) received the B.S. degree in electrical engineering from Yonsei University, Seoul, South Korea, in 2006, the M.S. degree in electrical engineering from the Korea Advanced Institute of Science and Technology, Daejeon, South Korea, in 2008, and the Ph.D. degree from the Department of Electrical and Computer Engineering and ElectroScience Laboratory, The Ohio State University, Columbus, OH, USA, in 2017.

In 2018, he joined the Ocean Surface Winds Team at the Center for Satellite Application and Research, National Environmental Satellite Data and Information Service, National Oceanic and Atmospheric Administration, College Park, MD, USA. Since 2020, he has been with the Hydrological Science Laboratory, NASA Goddard Space Flight Center, Greenbelt, MD, USA. He has also been with Global Science and Technology, Inc., Greenbelt, MD, USA, as a Support Scientist I/II. His research interests include satellite data calibration and validation, GNSS-R remote sensing applications, and active microwave remote sensing for soil moisture applications.

Rajat Bindlish (Senior Member, IEEE) received the B.S. degree in civil engineering from the Indian Institute of Technology, Bombay, Mumbai, India, in 1993, and the M.S. and Ph.D. degrees in civil engineering from the Pennsylvania State University, State College, PA, USA, in 1996 and 2000, respectively.

He was with USDA Agricultural Research Service, Hydrology and Remote Sensing Laboratory, Beltsville, MD, USA. He is currently with NASA Goddard Space Flight Center, Greenbelt, MD, USA. He is currently working on soil moisture estimation from microwave sensors and their subsequent application in land surface hydrology. He is a Science Team Member of NISAR, Aquarius, and GCOM-W missions. He is the Deputy Project Scientist with NASA's SMAP mission. His research interests include the application of microwave remote sensing in hydrology.

Dr. Bindlish is a Member of American Geophysical Union.

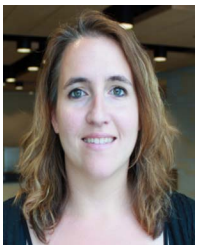

Alexandra Bringer (Member, IEEE) received the M.S and Ph.D. degrees in physics from the Université du Sud-Toulon-Var, La Garde, France, in 2009 and 2012, respectively.

Her studies were focused on physical oceanography and remote sensing. She started her career in the United States in 2014 when she joined the ElectroScience Laboratory, the Ohio State University, Columbus, OH, USA. She started working on microwave radiometry for cryosphere applications and on radio frequency interference detection and mitigation. She has continued to study those problematics when she was recruited to work for the NASA Goddard Space flight center, Greenbelt, MD, USA. She is currently with KBR Wyle, Houston, TX, USA, and with the NASA Goddard Space Flight Center, as a Research Scientist. She is also currently a member of the ATMS Science Team of the JPSS Mission and a Science Team member of the SMAP mission. Her research interests include Earth monitoring, microwave active and passive remote sensing for land, ocean and cryosphere applications and signal processing.

Dustin Horton (Graduate Student Member, IEEE) received the bachelor's degree in electrical engineering from the University of Alaska-Anchorage, Anchorage, AK, USA, in 2019. He is currently working toward the Ph.D. degree in electrical and computer engineering with the ElectroScience Laboratory, the Ohio State University, Columbus, OH, USA.

His research interests include remote sensing, electromagnetics, geophysics, and scientific product applications.

Joel T. Johnson (Fellow, IEEE) received the bachelor of electrical engineering degree from the Georgia Institute of Technology, Atlanta, GA, in 1991, and the S.M. and Ph.D. degrees from the Massachusetts Institute of Technology, Cambridge, MA, USA, in 1993 and 1996, respectively.

He currently serves as a Burn and Sue Lin Endowed Professor with the Department of Electrical and Computer Engineering and ElectroScience Laboratory, The Ohio State University, Columbus, OH, USA. His research interests include microwave remote sensing, propagation, and electromagnetic wave theory.

Dr. Johnson is a member of commissions B and F of the International Union of Radio Science, and a member of Tau Beta Pi, Eta Kappa Nu, and Phi Kappa Phi. He was the recipient of the 1993 best paper award from the IEEE Geoscience and Remote Sensing Society, National Science Foundation Career award, and PECASE award in 1997, and was recognized by the U. S. National Committee of URSI as a Booker Fellow in 2002. He was named an Office of Naval Research Young Investigator. He has served as Principal Investigator of the CubeSat Radiometer Radio Frequency Interference Technology Validation mission, as well as the Ultra-Wideband Software-Defined Microwave Radiometer for demonstrating airborne 0.5–2-GHz measurements of Earth surface thermal emission. He served as Technical Program Co-Chair of the 2017 International Geoscience and Remote Sensing Symposium, and currently serves as a Deputy Editor in Chief of IEEE TRANSACTIONS ON GEOSCIENCE AND REMOTE SENSING. He was also a past chair of the GRSS Technical Committee on Frequency Allocations in Remote Sensing.